INSTITUTE OF PHYSICS PUBLISHING JOURNAL OF PHYSICS D: APPLIED PHYSICS

J. Phys. D: Appl. Phys. **39** (2006) 1422–1426 doi:10.1088/0022-3727/39/7/013

Synchrotron high angular resolution microdiffraction analysis of selective area grown optoelectronic waveguide arrays

A Kazimirov[1], A A Sirenko[2], D H Bilderback[1], Z-H Cai[3], B Lai[3], R Huang[3] and A Ougazzaden[4]

[1] Cornell High Energy Synchrotron Source (CHESS), Cornell University, Ithaca, NY 14853, USA
[2] Department of Physics, New Jersey Institute of Technology, Newark, NJ 07102, USA
[3] Advanced Photon Source, Argonne National Laboratory, 9700 S. Cass Avenue, Argonne, IL 60439, USA
[4] Laboratoire Matériaux Optique, Photonique et Systèmes (MOPS), Université de Metz/Supelec, 57070 Metz, France

E-mail: ayk7@cornell.edu

Received 22 December 2005, in final form 2 February 2006
Published 17 March 2006
Online at stacks.iop.org/JPhysD/39/1422

Abstract
A synchrotron microbeam high-angular resolution diffraction setup based on a phase zone plate and a perfect Si(004) analyzer crystal was introduced to generate an x-ray microbeam with a lateral size of 0.24 μm and an angular resolution of 2 arcsec. The microbeam high angular resolution x-ray diffraction was applied to study InGaAlAs-based multiple quantum well (MQW) ridge-waveguide arrays produced by metal–organic vapour-phase epitaxy in a selective area growth regime with a central waveguide width varying from 1.6 to 60 μm. The analysis of the period T and the strain S in MQW ridge structures determined from the high-resolution diffraction data is presented. It was found that the MQW period is uniform across the ridge within the error bar of $\Delta T = \pm 0.25$ nm. Within the waveguide array, the MQW period and strain can be adequately described by a gas-phase diffusion model.

Remarkable progress in x-ray focusing combined with the high brilliance of the third generation synchrotron sources have made possible the production of sub-micron size beams for a variety of microdiffraction techniques [1]. Some applications, however, require not only a small size but also high angular resolution. For example, modern semiconductor technology traditionally depends on high resolution x-ray diffraction (HRXRD) in determining strain, composition, mosaic structure and defect density in thin epitaxial layers and the accuracy of this analysis is determined by the angular resolution of the x-ray setup [2]. In a typical macrobeam experiment, the required resolution is provided by a perfect crystal monochromator in front of the sample which serves as a beam conditioner. In a microbeam diffraction experiment with synchrotron radiation, the monochromator, typically double-crystal Si(111), is located upstream of the beamline and the angular resolution is determined by the numerical aperture of the focusing optics. The incongruity is obvious: focusing a beam to small size introduces a large divergence that ruins the angular resolution.

The current approaches to this problem are based on (1) a small size pinhole [3, 4], (2) a pinhole of a medium size and compressive crystal optics [5] and (3) a zone plate and a slit [6]. In [7, 8] we combined focusing optics (one-bounce imaging capillary) and post-focusing crystal (miniature Si(004) channel-cut) inserted in a limited space between the capillary and the sample to perform HRXRD and x-ray standing wave (XSW) measurements on InGaAsP microstructures grown by the selective area growth (SAG) technique. In this setup, a post-focusing collimating crystal made possible the excitation of a spatially confined XSW field with high visibility interference fringes inside the selected device structures. The advantages of our approach are (i) the use of a non-dispersive setup, thus relaxing requirements to the

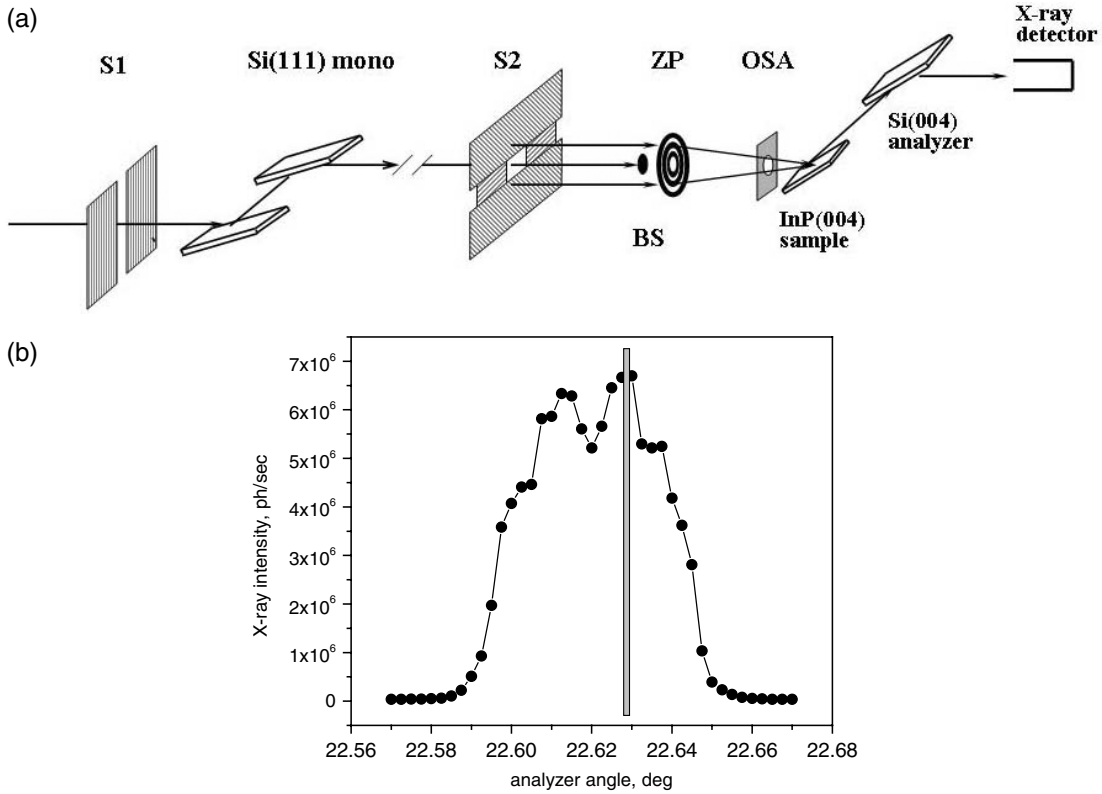

Figure 1. (*a*) Experimental setup. S1—upstream horizontal slit to limit horizontal source size; S2—vertical and horizontal slits in the hutch; BS—gold 30 μm diameter beam stop; ZP—phase zone plate with the outer zone of 0.12 μm and a focal distance of 149 mm and OSA—order sorting aperture. A single-bounce Si crystal analyzer provides a high angular resolution of about 2 arcsec. A scintillation counter measures the intensity of the x-ray beam diffracted from the sample and passed through the Si analyzer crystal. (*b*) Angular distribution of the focused beam intensity after the zone plate is measured by scanning the Si(004) analyzer crystal. Vertical band (width not to scale) shows the position of the acceptance window of the analyzer crystal.

monochromaticity of the incident beam, and (ii) the flexibility of controlling the angular resolution by means of the well-developed perfect crystal optics. When only the intensity of the diffracted beam has to be measured, this setup can be reversed, i.e. the collimating crystal providing angular resolution can be placed after the sample and can serve as an analyzer while the sample is illuminated by the convergent focusing beam. The setup based on an imaging capillary producing a 10 μm size beam and a three-bounce Si(004) analyzer crystal was used in our recent experiments on the InGaAlAs-based multiple quantum well (MQW) SAG structures with lateral size of 15 to 80 μm [9]. Here, we introduce the setup based on a phase zone plate and the Si(004) analyzer crystal producing an x-ray microbeam with a lateral size of 0.24 μm and an ultimate angular resolution of about 2 arcsec and apply it to study InGaAlAs-based MQW SAG structures grown by metal–organic vapour-phase epitaxy (MOVPE) in the SAG regime on InP(100) substrates.

The experiment was carried out at the APS 2ID-D diffraction microscope beamline [10]. The setup is shown in figure 1(*a*). The energy of the x-ray beam from the APS undulator was tuned to 11.890 KeV (above the As–K and below the Au–L edges) using a double-crystal Si(111) monochromator. A horizontal slit, S1, was used to limit the horizontal source size. The essential components of the setup are the phase Au zone plate, ZP, with an outer zone of 0.12 μm and the focal distance of 149 mm, 30 μm diameter Au beam stop, BS, an order sorting aperture, OSA, and a perfect Si(004) analyzer crystal mounted on a detector (2θ) arm of the six-circle diffractometer. The sample was mounted on a precision XYZ-translation stage. The angular distribution of the focused beam measured by the Si(004) analyzer crystal (figure 1(*b*)) shows the width of the beam incident on the sample to be 0.045° FWHM as determined by the angular aperture of the ZP. The angular position of the acceptance window of the Si(004) analyzer crystal at the angular position of the sample which corresponds to the InP(004) substrate peak is shown as a narrow vertical band. The maximum flux in our setup recorded by the scintillation detector with both the sample and the analyzer at Bragg position was $7 \cdot 10^6$ ph s^{-1}, which allowed us to collect diffraction data in a 20–30 min scan in an angular range of $\geqslant$2.5° with counting statistics sufficient for quantitative analysis.

The diffraction curve was measured by performing a $\Delta(\theta)$–$\Delta(2\theta)$ scan, where θ and 2θ denote rotation angles of the sample and the detector arm, respectively, and $\Delta(2\theta) = 2 \cdot \Delta(\theta)$, i.e. the angular deviation from the exact Bragg position of the analyzer is twice the one for the sample (for symmetric reflection). The angular resolution is determined by the acceptance range of the analyzer crystal 'intrinsic' rocking curve, i.e. 2.17 arcsec for the Si(004) crystal at 11.89 KeV. It is important to note that for the x-rays elastically scattered from the sample the analyzer crystal at any $\Delta(\theta)$–$\Delta(2\theta)$ angular position selects x-rays from the same part of the ZP angular

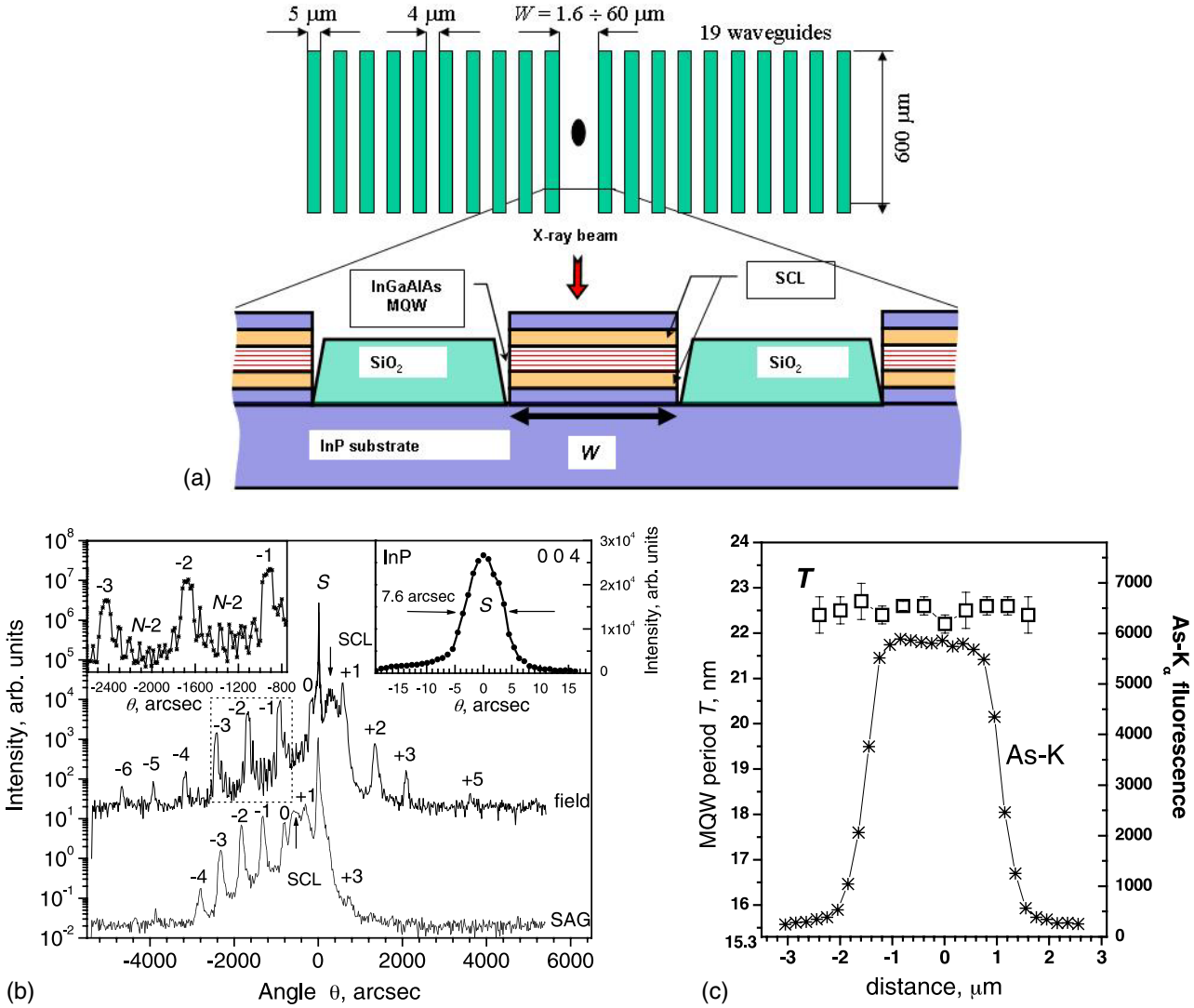

Figure 2. (*a*) Array of 19 waveguides. The InGaAlAs-based MQW structure with $N = 9$ periods and two SCLs form the active region of the waveguide. (*b*) Diffraction curve from the MQW in the 'field' region (upper curve) and from the centre of the 2.6 μm wide ridge waveguide (bottom curve). The MQW satellite peaks are marked according to their order. The right inset shows the substrate InP 004 peak (*S*) with FWHM = 7.6 arcsec. The left inset magnifies the superlattice peaks with clearly resolved (N-2) Kiessig fringes. The SLC peak is marked with arrow. (*c*) As–K_α fluorescence yield (right axis) and, determined from the HRXRD data, the MQW period T (left axis) across the waveguide ridge. Note that the As–K_α fluorescence data contains a contribution from the SLC layers as well. The $T = 15.3$ nm at the bottom of the left axis represents the 'field' value.

(This figure is in colour only in the electronic version)

aperture. Consequently, the shape of the angular distribution of the focused beam does not affect the measured diffraction curve. Therefore, the analyzer crystal, traditionally used in diffraction experiment to reduce contribution from diffuse and inelastic scattering from the sample, is used in our setup as an angular filter for the focused beam incident on the sample. For the sample with the angular distribution of the deformation fields of crystalline defects within the angular aperture of the zone plate, the measured diffraction curve is equivalent to a 'classical' double-crystal rocking curve measured with a wide open detector and a well-collimated incident beam. The size of the focused beam determined by scanning the 25 nm thick ZnO nanowire through the focal spot and measuring Zn–K fluorescence was 0.35 μm (vertical) $\times$ 0.24 μm (horizontal); the difference is due to different effective source sizes in vertical and horizontal planes. On the sample, the footprint of the beam in the diffraction plane was broadened by a factor of $1/\sin(\theta_B) \approx 2.8$. Below we discuss one of the applications of our experimental setup for the characterization of the Al-based optoelectronic device structures.

The MOVPE-SAG technique is a modern industrial technology for growing active elements of different optoelectronic devices simultaneously on the same substrate with the properties of these structures (such as strain and band gap) effectively controlled by the precise choice of the geometry of the SiO_2 mask [11–14]. We applied the microbeam HRXRD technique to study compositional and thickness variations in InGaAlAs-based waveguide arrays grown by MOVPE in the SAG regime in narrow openings between SiO_2 stripes (figure 2(*a*)). The InGaAlAs MQW

offers distinctive advantages over traditionally used and much better understood phosphorus-based InGaAsP structures due to a significantly larger conduction band gap offset [9, 15]. The active region of the waveguides was formed by an MQW with $N = 9$ periods and two 50 nm thick separate confinement layers (SCLs). In the field part of the wafer (far from the SiO_2 masks) the period of MQW is $T = 15.3$ nm and the composition of the 5 nm thick quantum wells and 10.3 nm barriers are $In_{0.65}Ga_{0.19}Al_{0.16}As$ and $In_{0.48}Ga_{0.19}Al_{0.33}As$, respectively, which corresponds to the MQW composite strain $S = +0.22\%$. These parameters have been determined from the HRXRD spectrum (figure 2(*b*), upper curve) using commercial RADS-Mercury BEDE software [16]. The width of the InP(004) substrate peak (figure 2(*b*), right inset), FWHM = 7.6 arcsec, with a theoretical intrinsic curve width of 4.83 arcsec and clearly observed $(N-2)$ Kiessig fringes between the superlattice peaks (left inset) demonstrate the excellent angular resolution of our setup. Using Ga–K and As–K fluorescence the microbeam was positioned and the HRXRD data were collected from the centre and across the selected waveguides.

Lateral vapour-phase diffusion and migration from the mask region are the two main mechanisms with different characteristic length scales which govern the SAG process and lead to thickness enhancement and compositional changes [12, 14]. We investigated specifics of the selective growth of semiconductor arrays with ridge widths smaller than the length of migration from the mask regions (MMR) of the metal–organic precursors in the MOVPE reactor which is typically of the order of 5 μm [14]. Based on the HRXRD data we determined the thickness and the strain in the central element of the waveguide structures with different width W and the changes in these values in different elements of the same array to compare the properties of the micron-wide SAG structures ($W \leqslant 5\,\mu$m) with that of the conventional ones ($W \geqslant 10\,\mu$m).

The HRXRD spectrum measured in the centre of the 2.6 μm-wide ridge waveguide is shown in figure 2(*b*), bottom curve. The period increased to $T = 23.5$ nm and the composite strain changed to $S = +1.1\%$ with the thickness and the strain of the separate well and barrier layers being $T_W = 9$ nm, $T_B = 14.5$ nm, $S_W = 2.5\%$ and $S_B = 0\%$, correspondingly. The cross section analysis (figure 2(*c*)) shows that the MQW period T is uniform across the ridge to within the error bar of $\Delta T = \pm 0.25$ nm. This result has important practical implications for the growing of uniform micron wide Al-based ridges without the need for etching the overgrowth edges, an unavoidable technological step in the production of the P-based SAG structures.

Variation of the MQW parameters with the width of the central waveguide W is shown in figure 3. Measurements were taken in the centre waveguide while the parameters for the other ridges and the total oxide mask width (10 μm × 5 μm = 50 μm) on both sides of the central waveguide are the same for all arrays. To understand better the main mechanisms of the observed changes, a 3D vapour phase diffusion model [13] with effective diffusion lengths, $\boldsymbol{D_v/k}$, of metal–organic precursors as fitting parameters was used to fit the data. The best fit (solid line) yielded values of $\boldsymbol{D_v/k}(\mathrm{In}) = 36\,\mu$m and $\boldsymbol{D_v/k}(\mathrm{Ga}) = 130\,\mu$m, which are consistent with [13] and our previous studies [9]. This result shows that the SAG growth in

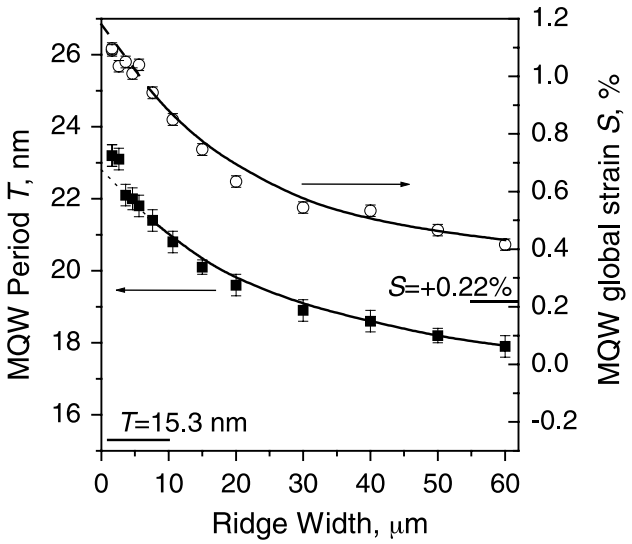

Figure 3. The MQW period T (filled squares, left axis) and the composite strain S (opened circles, right axis) in the central waveguide as a function of the ridge width W. Solid curves are results of the vapour phase diffusion model calculation with $\boldsymbol{D_v/k}(\mathrm{In}) = 36\,\mu$m and $\boldsymbol{D_v/k}(\mathrm{Ga}) = 130\,\mu$m for the ridge width range between 10 and 60 μm. Dashed lines are the guide to the eye for narrow ridges.

waveguide arrays can be adequately described by the gas-phase diffusion model for the ridge widths $W > 10\,\mu$m. Analysis of our experimental data for narrow ridges ($W < 10\,\mu$m) requires further refining of our model taking into account contributions of the short-length diffusion processes, such as MMR effect and surface diffusion [14]. However, since the observed additional growth enhancement in the most narrow ridges with $W = 1.6$ and 2.6 μm (dashed curves in figure 3) does not show any significant deviations from the smooth behaviour described by the gas-phase diffusion model (solid curves in figure 3), we can predict that the MMR effect for the strain and thickness enhancement in Al-based SAG structures is weak compared with the gas-phase diffusion SAG effect.

Figure 4 shows variation of the composite strain and period for different elements of the waveguide array with all ridges of the same width $W = 4\,\mu$m. The MQW period T and strain S are uniform for the central elements and decrease towards the edge of the array approaching the field values at a distance of about 50 μm from the edge. Note a narrower transient region and a wider plateau for the global strain S. The cross-sectional profile of the As–K_α fluorescence (top panel) is proportional to the total thickness and agrees very well with the period T determined from the HRXRD data. The characteristic distance between the edge of the array and the uniform region in the centre correlates well in this work with the measured diffusion length $\boldsymbol{D_v/k}(\mathrm{In}) = 36\,\mu$m in the gas phase. This result is important when these arrays are integrated into monolithic optoelectronic device, e.g. as wavelength filters.

In conclusion, an x-ray setup based on phase zone plate and perfect analyzer crystal was introduced, which is capable of producing x-ray microbeam with a lateral size of 0.24 μm and an angular resolution of about 2 arcsec. High angular resolution was provided by the analyzer crystal while the

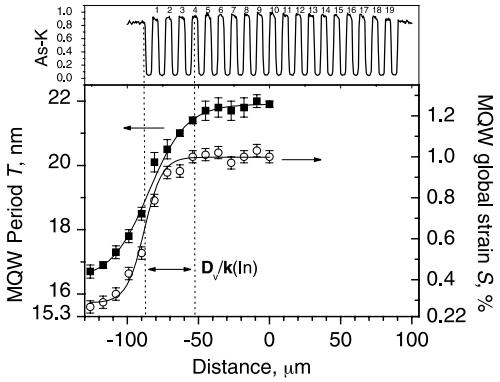

Figure 4. The period (■) and the strain (○) in different elements of the micro-waveguide array and in the open area of the wafer. The bottom of the plot corresponds to the 'field' values $T = 15.3$ nm and $S = +0.22\%$. The solid curves guide the eye. Two vertical dotted lines confine the area of the first four ridges where the properties change more rapidly. Estimated value of the In precursor diffusion length $\boldsymbol{D}_v/\boldsymbol{k}(\mathrm{In}) = 36\,\mu$m is shown for comparison by the double arrow. The As–K_α fluorescence yield proportional to the total thickness (MQW + two SCL) is shown in the upper panel.

sample is illuminated by a highly convergent beam from the focusing optics. The high brilliance of the third generation synchrotron source allowed enough intensity to collect high resolution diffraction data in a wide angular range within a reasonable amount of time. The setup was applied to study InGaAlAs-based MQW waveguide arrays grown by MOVPE in the SAG regime with the size of the central waveguide ridge varying from 1.6 to 60 μm. Cross-sectional analysis revealed a uniform MQW period across the ridge providing important evidence in favour of the Al-based optoelectronics technology as an alternative of the traditionally considered P-based one.

Acknowledgments

We thank V Gupta and K Bacher for MOVPE growth. The use of the Advanced Photon Source was supported by the US Department of Energy, Office of Science, Office of Basic Energy Sciences, under Contract No W-31-109-ENG-38. The Cornell High Energy Synchrotron Source was supported by the National Science Foundation and the National Institutes of Health/National Institute of General Medical Sciences under award DMR-0225180.

References

[1] Riekel C 2000 *Rep. Prog. Phys*. **63** 233–62
[2] Bowen D K and Tanner B K 1998 *High Resolution X-ray Diffractometry and Topography* (London: Taylor and Francis)
[3] Cai Z-H *et al* 1999 *Appl. Phys. Lett.* **75** 100
[4] Eastman D E, Stagarescu C B, Xu G, Mooney P M, Jordan-Sweet J L, Lai B and Cai Z 2002 *Phys. Rev. Lett.* **88** 156101
[5] Kimura S *et al* 2000 *Appl. Phys. Lett.* **77** 1286
[6] Kimura S, Kagoshima Y, Koyama T, Wada L, Niimi T, Tsusaka Y, Matsui J and Izumi K 2004 *AIP Conf. Proc.* **705** 1275
[7] Kazimirov A, Bilderback D H, Huang R and Sirenko A 2004 *AIP Conf. Proc.***705** 1027
[8] Kazimirov A, Bilderback D H, Huang R, Sirenko A A and Ougazzaden A 2004 *J. Phys. D: Appl. Phys.* **37** L9
[9] Sirenko A A,Kazimirov A, Huang R, Bilderback D H, O'Malley S, Gupta V, Bacher K, Ketelsen L J P and Ougazzaden A 2005 *J. Appl. Phys.* **97** 063512
[10] Cai Z, Lai B and Xu S 2003 *J. Phys. IV* **104** 17
[11] Van Caenegem T, Moerman I and Demeester P 1997 *Prog. Cryst. Growth Charact.* **35** 263
[12] Gibbon M, Stagg J P, Cureton C G, Thrush E J, Jones C J, Mallard R E, Pritchard R E, Collis N and Chew A 1993 *Semicond. Sci. Technol.* **8** 998
[13] Alam M A *et al* 1999 *Appl. Phys. Lett.* **74** 2617
[14] Sakata Y, Inomoto Y and Komatsu K 2000 *J. Cryst. Growth* **208** 130
[15] Adachi S 1992 *Physical Properties of III–V Semiconductor Compounds* (New York: Wiley)
[16] Wormington M, Panaccione C, Matney K M and Bowen K D 1999 *Phil. Trans.: Math. Phys. Eng. Sci.* **357** 2827